Direct measurement of elastic modulus of InP nanowires with Scanning Probe Microscopy in PeakForce QNM mode

P Geydt[1*], M Dunaevskiy[2, 3], P Alekseev[2], J-P Kakko[4], T Haggrén[4], E Lähderanta[1] and H Lipsanen[4]

[1] Laboratory of Physics, Lappeenranta University of Technology, 53851 Lappeenranta, Finland
[2] Ioffe Physical Technical Institute, RAS, 194021 Saint-Petersburg, Russia
[3] National Research University of Information Technologies, Mechanics and Optics (ITMO), Saint-Petersburg 197101, Russia
[4] Department of Micro- and Nanosciences, Micronova, Aalto University, P.O. Box 13500, FI-00076 Aalto, Finland

*Corresponding author's email: Pavel.Geydt@gmail.com

Abstract. In this manuscript, we present the study of elastic properties of InP nanowires with help of scanning probe microscope in advanced PeakForce Tapping® regime. The measuring method was developed in order to investigate the Young's modulus of these cone-shaped structures with significant accuracy. The difference in InP elasticity for wurtzite phase and zinc-blende phase was revealed. It was shown that elastic modulus of InP nanowires significantly increases from 60 GPa to more than 100 GPa when diameter of a nanowire is reduced below 50 nm. The core-shell model for InP nanowire was used for the explanation of this effect.

1. Introduction

Due to the worldwide increase of electric power demands and modern requirements for clean energy, much attention is paid to renewable Solar technologies. For example, the photovoltaic cell covered with semiconductor nanowires (NWs) is an interesting architecture proposed for next-generation Solar energy panels [1]. Its diverse designs and characteristics are extensively studied with significant attention to features of their electrical conductivity [2], surface states and charge trapping effects [3], type and uniform properties of shell passivation material [4] and necessary level of doping [5]. Additionally, it is vital to consider the NW's mechanical strength [6], since nanowires need to be covered by viscous transparent protective layer and withstand operational stresses under temperature expansion.

While electric properties of the NW array can be partially tested with a massive pad (i.e. a microplate electrode), it is still difficult to access the NWs individually. Seemingly, only awareness of all mentioned parameters of individual NW can help to design and develop NW-based devices. Although, measuring their elastic properties in contact appears even more laborious and accessible only by devices enabling nanoscale resolution. Among all available mechanical parameters, specifically the Young's modulus is the most important criterion, because it characterizes the preservation of technological quality of the NWs considering their reversible deformations.

Multiple publications describing tools and methods to study the elastic characteristics of one-dimensional systems have been recently published [7 - 10]. Moreover, few works were focused on semiconductor nanowires, e.g. ZnO [11] and GaAs [12], but surprisingly no reports revealed the elastic

properties of InP NWs. In fact, InP is considered more advantageous, e.g. for Solar cells, due to the reduced density of surface states [13]. Capability to produce photocurrent for InP NW-based cell has recently been extended above efficiency of 13% [14] and further beyond theoretical expectation of efficiency limit [15]. It should also be noted, that crystal structure of InP NWs can be either wurtzite (WZ) or zinc-blende (ZB), which was confirmed by electron diffraction experiments. Wurtzite InP is an exotic material, whose elastic properties have not been experimentally studied yet. We suggested semicontact Scanning Probe Microscopy (SPM) as a proper tool for this investigation.

Considering the previously collected experience on difficulties with positioning, calibration and interpreting of the data, we would like to report our experimental results for the measurements of elasticity of inclined cone-shaped InP NWs, obtained with PeakForce Tapping® mode SPM. In this manuscript, our observations over two series of InP NWs with wurtzite crystal structure and zinc-blende structure will be demonstrated with suggestions concerning the usage of PeakForce measuring method.

2. Sample preparation and Experiment

The arrays of inclined nanowires were fabricated by vapour-liquid-solid (VLS) mechanism in metalorganic vapour phase epitaxy (MOVPE) chamber. Golden droplets with diameter ~20 nm were sputtered on hot silicon substartes, followed by controlled growth of conical InP NWs. The growth direction, diameters and lengths of the nanowires were controlled by duration of vapour source flow and temperature regime. Thickness of obtained InP NWs appeared gradually declining from approximately 160 nm for diameter of a lower base to approximately 20 nm for diameter of an upper part, i.e. near the Au caps. Lengths of InP NWs were approximately 3 μm while distance between adjacent structures exceeded value of 3 μm to secure them from unintentional encounter. NWs were not intentionally doped in order to study the properties of genuine InP material.

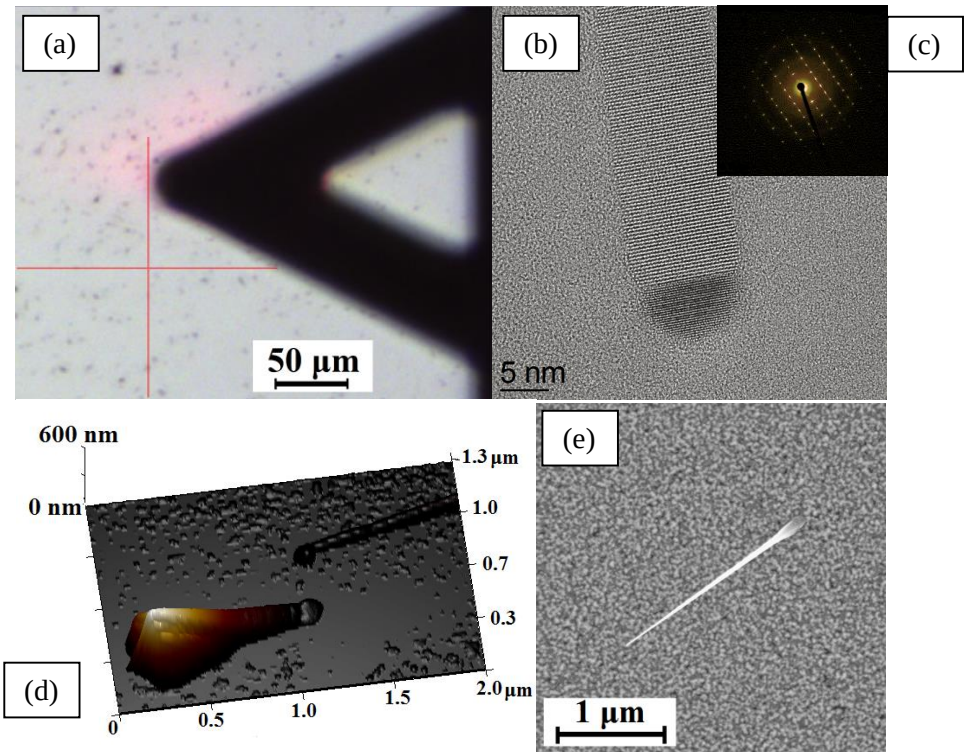

Figure 1. (a) Optical image of an array of InP NWs at magnification 200x with A-shaped SPM cantilever and reflection spot of scattered red laser beam. (b) HRTEM image of wurtzite InP NW near the Au cap, and inset (c) presenting the corresponding electron diffraction pattern for WZ InP phase. (d) 3D SPM image of inclined InP NW and a broken NW lying nearby on the substrate. (e) SEM image of inclined InP NW, where the conical shape and a lower "thick base" are distinguishable.

Crystal structure and sizes of InP NWs were investigated by scanning electron microscope (SEM), transmission electron microscope (TEM) and scanning probe microscope (SPM) (See Figure 1). It should be noted, that NWs had specific "thick bases" at the growth contact point on the wafer (seen on Fig. 1 (d)), so their lever's length (leg of bending) for further correct calculation of elasticity should be reduced by approximately 0.2 micron (See the lower part of the NWs on Fig. 1 (d) and Fig. 2). All SPM measurements were performed in standard room conditions without intentional sample's pretreatment.

Experimental setup

At first, it may be emphasized, that NWs can be observed and targeted even with help of standard optical microscope with magnification 100x. It does not seem possible to detect the NW's structure and geometry in details, but location of single freestanding nanoobject can be noticed as one or two dark pixels revealed by the sensitive matrix of the optical microscope OMV Nikon coupled with BRUKER Multimode 8 microscope used in our work. Due to the distinctive distance between the NWs, it was possible to distinguish separate individual NWs having length ~3 μm with only tens of nanometers in cross-section (See black spots on Fig. 1 (a)). Reason here is associated with distortion of light by such "surface defect" (i.e. NW) mounted on the smooth flat wafer's surface having roughness ~1 nm for 10x10 μm^2. Later these NWs were successfully targeted with SPM probe, considering the known geometry of the probe tip in such a way that tip's apex was engaging the sample's surface successfully already in few microns to the certain desired NW.

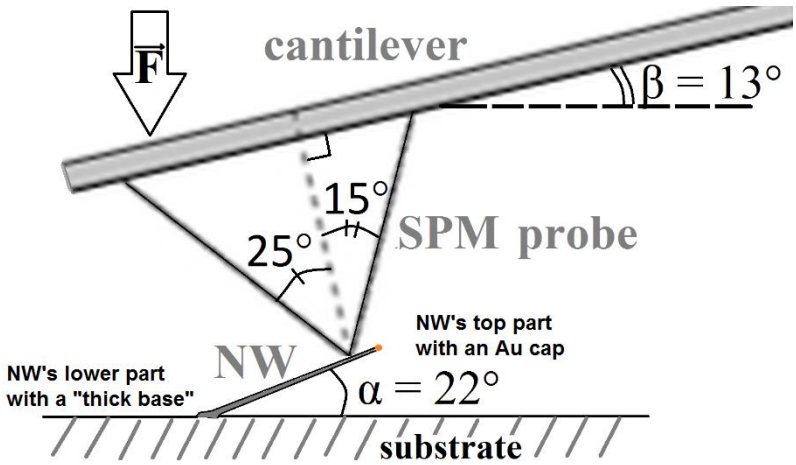

Figure 2. Experimental scheme reflects the realistic scale for SPM probe above inclined InP NW mounted on the wafer and corresponding angles of their contact interaction. The specified angles α ~ 22° and β = 13° are being reduced upon increasing of the bending force *F* in our experiment.

Schematics of the measuring setup is shown on Figure 2. The incline angle of an SPM cantilever mounted in a probe holder is 12°. Addition to bending angle ≈1° is specified by the manufacturer (Bruker Inc.) for the SPM probes used in this study. NW-substrate angle α was ~22°.

Methodic of the measurements

Elastic properties of inclined NWs were studied previously by the "multiple points method" (also called as method of "Force-Load curves") [12]. The main advantages of this method are that it can be operated on most of the SPM systems and it provides data considerably fast. However, this method requires precise knowledge of the lever distance from the NW's base, while it seems difficult to determine the coordinates of "fixing point", where the NW's lower base begins to be detached from the wafer. Moreover, small amount of data points in one experimental cycle is a significant drawback from the viewpoint of repeatability of these measurements.

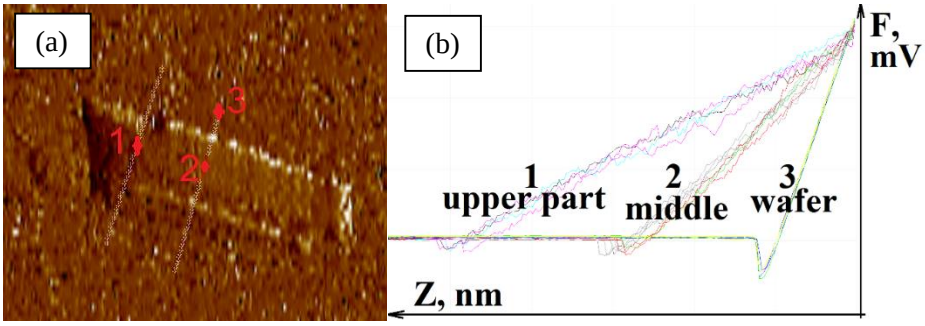

Figure 3. Multiple points method of studies allowed obtaining the data values of elasticity. (a) SPM image of inclined InP NW; (b) *F(z)* force-load curves measured at the substrate (3) and at the upper (1) and middle (2) parts of the NW, corresponding to certain NW's lever lengths.

The measurements of force-load curves *F(z)* can be performed only in a limited amount of positions (See Figure 3), due to the sample drift and lateral bending of the nanostructure, causing moderate accuracy. Moreover, the uncertainty of location of lever base's starting point causes additional error in the calculated elastic modulus, leading to decrease of preciseness of each measurement. The force-load curves measurements were used only for comparison of data with the elasticity measured with PeakForce mode. Still, force-load curves provided strong correlation of results at least by the order of values with Young's modulus of the InP NWs from PeakForce mode.

Utilization of the PeakForce QNM mode

From emergence of the PeakForce Tapping® technique in 2009 it became possible to make quantitative force estimations after processing the data of SPM experiments, even for fragile samples, e.g. standing NWs. Later, with the help of newer PeakForce Quantitative Nanomechanics (QNM) mode [16] it became possible to obtain values of elastic modulus in the range between 100 Pa - 20 GPa simultaneously with mapping of a material's surface Topography. Method provides eight data channels simultaneously to diversely describe the samples (See Figure 4). Unfortunately, even QNM cannot be applied to straightforward study of the Young's modulus of inclined NWs, because "Deformation" data used in calculation of DMT elastic modulus channel (based on Derjaguin-Muller-Toporov model of elastic contact) would represent the bending of a NW instead of the material's Deformation. However, there is a way to calculate the proper elastic modulus, if a spring constant of the SPM cantilever would be accounted with correct lever length and precisely registered force of probe-sample interaction.

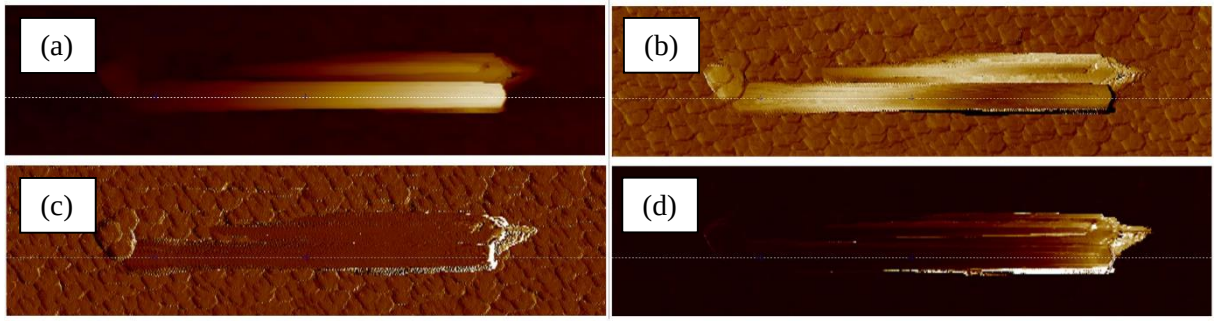

Figure 4. SPM images of inclined InP NW, with lower base on the left. Comparison of data from PeakForce mode channels used to quantify the elasticity: (a) Topography, (b) PeakForce, (c) PeakForce Error and (d) Deformation. Image sizes are 3x0.75 μm. PeakForce Setpoint was normalized to 0.2 nN, while distinct color gradient on (b) is further explained on Figure 5.

At the start, we calibrated the cantilever's spring constant k_{Probe} and the SPM photodetector's deflection sensitivity for relatively soft cantilevers. SPM probe was chosen experimentally from the probes with spring constants *k* in the range 0.06 - 2.80 N/m. For example, the "SCM-PIT" cantilever's *k* was evaluated as 0.438 N/m by the calibration protocol. Probe tip was coated by manufacturer with electrically conductive metal layer, so the tip's apex was wide enough (tip radius > 20 nm) to establish a stable contact and decrease the sliding effect away from the NW's sloping surface. Then, one of the NWs which was oriented towards the SPM cantilever was chosen from the OMV and Topography imaging, and imaging area was additionally rotated by few necessary degrees in such a way that "fast scanning direction" of the SPM met the NW's long axis, i.e. the profile of the plane of bending down movement. It is important that NW's base should be situated on the left of the image when cantilever is on the right (as seen on Fig. 1), so that inclination of the NW ($\alpha = 22°$) should partly compensate the inclination of the SPM cantilever ($\beta = 13°$) (See scheme on Fig. 2). Thus, data channels for tip movement direction from left to right become sources of valuable data for further calculations. It is required to establish the negligible sample drift achievable by constant temperature and measurements started always from the same side of the scan image, e.g. up or down. Otherwise, it seems beneficial to fix the "slow scanning direction". Lateral resolution of the scans was 1024x100 for scan size 3x0.375 micron, so that at least one of the horizontal profile lines would have a width ~4 nm which is considerably smaller than diameter of the NWs. This was considered important for eliminating of the parasitic sliding effect when SPM tip does not properly track the upper face of the inclined NW. Here we need also to highlight that fabricated NWs appeared to have a conical shape instead of cylindrical, which was considered by adding $\gamma \approx 1.5°$ of cone angle to numerical model of the NW's shape and bending, additionally correcting the Young's modulus measurement.

3. Results

Series of recorded profiles for necessary data channels (i.e. Topography, Deformation and Peak Force) were used for calculation of inverted spring constant $1/k(L)$ along the NW's length *L*, when Deformation channel was divided by the corresponding measured Peak Force channel values (*PF*) (See horizontal profile lines on Fig. 4). PeakForce mode indicates a deviation from the ideal presetted force parameter (i.e. Setpoint), which is recorded separately as Peak Force Error channel. Topography channel (correspondent to height of the structure under applied bending force) provided us information about the height profile line of our interest (See Fig. 4(a)) and about the location of the NW lever's beginning.

To additionally increase the accuracy of our measurements, we summarized data for following bending forces applied to the NWs: 100 pN, 200 pN, 500 pN, 1 nN, 2 nN, 5 nN, 10 nN, 20 nN, 50 nN, 100 nN and 200 nN. These three orders of magnitude in range of the utilized Setpoint force of probe-sample interaction led to few distinctive observations. Firstly, bending of the NW (controlled by Topography and Deformation) is linearly dependent from the *PF* in the areas, where spring constants of a NW and a cantilever were comparable. Secondly, increasing of the force did not affect the shape of the Peak Force channel profile line *PF(L)* on the area where it was acquired, while curves had same features further described in Section 3.2. Finally, increasing of the force to extensive Setpoint values above 20 nN did not lead to non-linear deformations inside the NW. Instead of reaching the shear strain value and irreversibly deform the structure, the SPM probe slided off from it, and NW further became bended in lateral plane. This resulted in observation that the displayed form of the NW was observed thinner at the NW's top part on certain extent depending from the force. We did not account the profile area where bending was unstable and indicated lateral movement. Therefore, even for the relatively high value of the force F = 50 nN we were able to obtain a shortened profile of the NW without the segment responsible for the upper part of the NW. Forces above 100 nN were used simultaneously with increasing the PeakForce tapping amplitude (from 150 nm to 300 nm) only to brake the NWs. A broken NW lying on a smooth wafer (Seen on Fig. 1(d)) provided us with information about the NW's conical shape *D(L)* and the cone angle $\gamma \approx 1.5°$. In such a procedure, NWs did not fly off far from the growth location, but were securely attached to the wafer by the van der Waals forces and surface adhesion.

In order to improve preciseness of our calculations, diameters of the NWs were primarily controlled by averaging the SEM data for separate NWs in an array, then compared and proofed on each certain

broken NW (by the Topography profile on smooth wafer surface), and finally verified for each NW by modeling auto fit of calculated parameter of middle diameter D_{mid}. Thereby, diameter still could be slightly enlarged, which correlates with RMS roughness of the wafer surface ~5 nm for 5x5 μm^2 area (See Fig. 1 (d)) and insignificant own roughness of the NWs. Although, summarized estimation of this error for values of middle diameter D_{mid} is approximately 1 nm.

Processing of the acquired PeakForce data and curves

It should be specified, that synchronization time moment (Sync parameter) needs to be manually corrected to perform correct PeakForce QNM measurements of a highly bendable structure. It is explained by the fact that cantilever requires additional time to reach the lowest (bended) position. Thus, "*Sync distance New"* parameter must be manually designated to be close or equal to "*Sync distance QNM"* parameter, which cannot be achieved by *Autoconfig* feature of NanoScope SPM software. The value would be adjusted from ~77.5 msec to ~84 msec, correspondingly with the Setpoint force, when it is being increased from 0.5 nN to 50 nN. Otherwise, all parameters of a PeakForce curve would be estimated for incorrect moment of time. Unfortunately, this time-shift can only be found experimentally for each individual NW and force. It cannot be adjusted properly beforehand, since SPM probe's first engagement with the sample is done usually on the spacious area of the hardly deformable wafer. We have further intention to develop such calibration procedure of Sync parameter in the SPM's software.

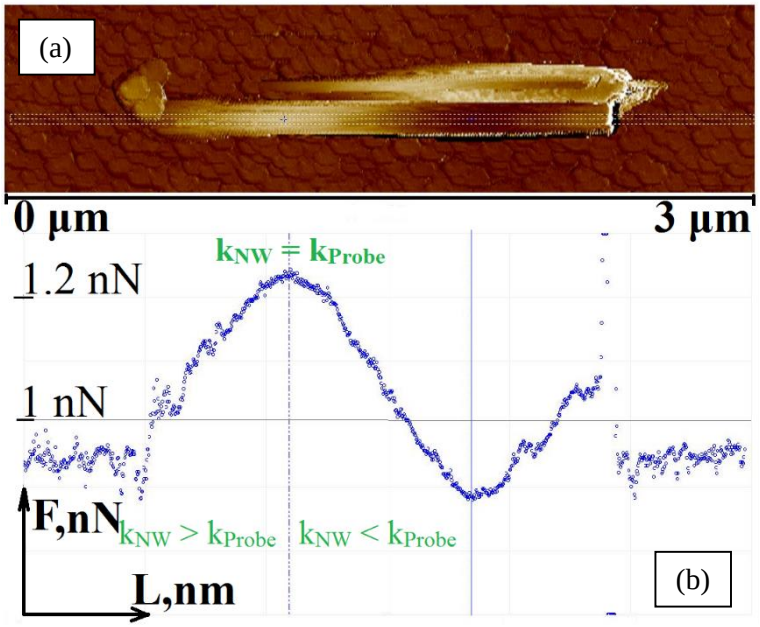

Figure 5. (a) Peak Force data channel and (b) corresponding *PF(L)* values for the bended InP NW. PeakForce Setpoint was normalized to 1 nN. The curve represents 1024 data points of elasticity over one line. It should not be confused with the PeakForce curve itself associated with only one data point.

As can be seen from the curve on Figure 5 read from left to right, negligible noise level is noticed for wafer and this deviation is further recorded into the Peak Force Error channel. Then SPM probe starts to tap on the stiff base of the NW, which can not be deformed by the soft probe. The microscope's feedback controller system preliminary increases the force applied in every measurement point of the elevated base. Deformation here is solely related with bending of the cantilever ($k_{NW\_base} >> k_{Probe}$). Then a bending lever is approached, which causes a gradual increase of the measured *PF* value, but the nanostructure is still stiffer than cantilever ($k_{NW} > k_{Probe}$). Increase of the presented curve is the result of the lever rule, and at distinct moment this curve have maxima. Here the spring constants are equal and Deformation registered by SPM photodetector is divided equally between bending deflection of the SPM

cantilever and the NW's bending (**$k_{NW} = k_{Probe}$**). It should be noted, that according to the QNM calibration requirements specified by the device manufacturer, the PeakForce QNM mode is capable to measure the Young's modulus when stiffness of the probe is equal or similar to stiffness of the measured material. Actual informative bending of the NW occurs mainly on the right from the maxima, i.e. in the region where the NW is softer then the cantilever ($k_{NW} < k_{Probe}$). Then curve decreases further until the minima, where sliding becomes predominant and measurement is not stable anymore. The more right part of the curve represents bending of the SPM cantilever's base back side and one spike due to the short encounter with side plane of the cantilever. Thereafter, one can conclude that only limited part of the *PF(L)* curve, i.e. slope closer to the area where spring constants are equal, should be used to calculate the k_{NW} and the resulting elastic modulus. Still, it was already enough to obtain more than 300 data points from the profiles for each applied force. Then, the following formula (1) valid for calculation of stiffness of the conical balk (with round section) was used to calculate the Young's modulus *E* of the NWs:

$$\frac{Deformation}{PF} = \frac{1}{E}\frac{4}{3\pi}\frac{16}{D_{mid}^4}\frac{x^3}{(1+a(2x-L))(1-aL)^3} \quad (1)$$

Here D_{mid} is the average diameter of the nanowire, *L* is the length of the nanowire, $a = \gamma/D_{mid}$ is a conical factor associated with a cone angle γ, and *x* is a coordinate of the SPM probe's contact with the nanowire.

Summarizing the elastic strength of the InP nanowires

Finally, we can compare the calculated elastic modulus data for 10 different NWs in Table 1, where first five values are shown for ZB, latest five are given for WZ. Corresponding error values are based primarily on inaccuracy of the measured diameters of the NWs. In our model, elasticity was estimated for the point of middle diameter D_{mid}, i.e. approximately near the middle of a NW. Its location was found from the *D(L)* profile for already broken NW, and it was also situated on the linear slope of *PF(L)* curve (See Fig. 5(b) where $k_{NW} < k_{Probe}$), and further proofed by model fitting. Since diameter *D(L)* is linearly dependent from the length *L*, so *PF*(*L*) ≡ *PF*(*D*), and *E* is a property of a NW's material.

Table 1. Estimated values of Young's moduli for 10 measured ZB and WZ InP NWs.

	Middle diameter, nm	**Young's modulus, GPa**	Estimated Error, GPa
ZB series	60	60	25
	60	54	20
	54	70	30
	50	150	60
	50	80	30
WZ series	50	105	40
	42	170	70
	40	230	90
	40	340	130
	36	250	100

Young's modulus for InP ZB bulk material is known to be 61 GPa. This was approved experimentally for ZB InP NW with middle diameter >80 nm. However, according to our results, elasticity of the InP material increases with decreasing of NW diameter. Partly this can be explained in terms of the core-shell model, previously used to explain similar trend for GaAs [11] and ZnO [12] nanowires. In fact, shell atoms are dominating in the properties with decreasing of the diameter of the NWs less then ~50 nm, so stiffness of the nanostructure increases, if surface material is rigid.

Thus, it seems that shell material of InP NWs is stiffer than its core. This effect can be partially associated with properties and amount of oxidized surface material in the overall volume of the NW, since NWs were kept in air for two months before the experiments. However, the drastic difference in elasticity was observed specifically between WZ and ZB phases of InP NWs, and we were able to convince that WZ phase of InP gives strongly rigid contribution to the elastic properties of InP material.

4. Conclusions

We made measurements of elasticity of InP NWs with relatively new experimental method and developed a protocol for data treatment, which gave highly reproducible data. This can be qualified as an attempt to make reproducible accurate and fast tests with SPM in PeakForce QNM mode, which can be further used to organize a SPM-based station for assessment of elasticity of versatile bendable 1D structures. Elastic modulus of InP NWs was studied for the first time. Moreover, Young's modulus of wurtzite InP has been obtained for property indexing issues for the first time. Results show that wurtzite InP NWs are at least two times stiffer than zinc-blende InP NWs. Young's modulus increases when material's size decreases, which was observed for the NWs with diameters less than 50 nm. These considerations are proposed to improve design and characterization of NW-based structures.

References

[1] Parkinson P, Lee Yu-H, Fu L, Breuer S, Tan H and Jagadish Ch 2013 *Nano Lett.* **13** 4
[2] Duan X, Huang Yu, Cui Y, Wang J and Lieber C M 2001 *Nature* **409** 6816
[3] Mikkelsen A and Lundgren E 2013 *Surf. Sci.* **607**
[4] Vugt L K, Veen S J, Bakkers E P A M, Roest A L and Vanmaekelbergh D 2005 *J. Am. Chem. Soc.* **127** 35
[5] Zhang W, Lehmann S, Mergenthaler K, Wallentin J, Borgström M T, Pistol M-E and Yartsev A 2015 *Nano Lett.* **15** 11
[6] LaPierre R R, Chia A C E, Gibson S J, Haapamaki C M, Boulanger J, Yee R, Kuyanov P, Zhang J, Tajik N, Jewell N and Rahman K M A 2013 *Phys. Stat. Sol. RRL* **7** 10
[7] Song J, Wang X, Riedo E and Wang Z L 2005 *Nano Lett.* **5** 10
[8] Stan G, Ciobanu C V, Thayer T P, Wang G T, Creighton J R, Purushotham K P, Bendersky L A and Cook R F 2009 *Nanotechnology* **20** 035706
[9] Gordon M J, Baron Th, Dhalluin F, Gentile P and Ferret P 2009 *Nano Lett.* **9** 525
[10] Kushima A, Huang J Yu and Li J 2012 ACS Nano **6** 11
[11] Chen C Q, Shi Y, Zhang Y S, Zhu J and Yan Y J 2006 *Phys. Rev. Lett.* **96** 075505
[12] Alekseev P A, Dunaevskii M S, Stovpyaga A V, Lepsa M and Titkov A N 2012 *Semiconductors* **46** 641
[13] Mohan P, Motohisa J and Fukui T 2005 *Nanotechnology* **16** 2903
[14] Wallentin J, Anttu N, Asoli D, Huffman M, Åberg I, Magnusson M H, Siefer G, Fuss-Kailuweit P, Dimroth F, Witzigmann B, Xu H Q, Samuelson L, Deppert K and Borgström M T 2013 *Science* **339** 6123
[15] Krogstrup P, Jørgensen H I, Heiss M, Demichel O, Holm J V, Aagesen M, Nygard J and Morral A F 2013 *Nature Photonics* **7** 4
[16] Sahin O and Erina N 2008 *Nanotechnology* **19** 445717